Preheat Strategy of a Molten Salt Test Receiver

Isabell Reisch[1,a)], Cathy Frantz[1)], Miriam Ebert[1)],Matthias Binder[2)], Christian Schuhbauer[2)]

[1] *German Aerospace Center, Institute of Solar Research, 70569 Stuttgart, Germany*
[2] *MAN Energy Solutions SE, 94469 Deggendorf, Germany*
[a)] *Corresponding author: isabell.reisch@dlr.de*

Abstract. Due to the high crystallization point of 240 °C of the solar salt used as a heat transfer media in solar tower power plants, all pipes that are carrying the molten salt must be preheated to prevent the solidification of the solar salt and thus plugging and damaging the pipes. In commercial power plants the preheating of the pipes is mainly done electrically by using conventional resistance heaters. Due to the high incident solar radiation during solar operation, this approach cannot be used for preheating the absorber tubes of the receiver. Instead, the receiver will be preheated by the reflected energy of the sun. In order to ensure a frictionless start of the plant a preheat strategy must be developed that leads to a homogeneous temperature distribution independently of the day in the year, the time of the day and of the ambient conditions. For the preheating strategy of the HPMS-II test receiver several boundary conditions were defined; the most important being: The receiver must reach a target temperature of 350 °C and have to maintain the maximum temperature ramp of 30 K/min specified by the absorber coating producer. Within the scope of this paper, an optical and thermal simulation model of the solar preheat strategy for an external molten salt test receiver was developed and the preheating strategy was simulated.

STATE OF THE ART

State of the-art CSP receivers reach outlet temperatures up to 565 °C [1]. Within the HPMS-II project, the receiver system is pressurized with synthetic air, so that the molten salt (sodium nitrate ($NaNO_3$) 60 % wt. and potassium nitrate (KNO_3) 40 % wt.) remains stable at higher temperatures, thus enabling the receiver outlet temperature to be increased to up to 600 °C [2]. This leads to a higher steam cycle efficiency, a decrease in storage and steam generator size and thus a decrease of the levelized cost of electricity (LCOE) accordingly [3]. This test receiver will be implemented in the multi focus tower in Jülich, Germany. Before the cold absorber tubes of the receiver can be filled with the hot Solar Salt, the absorber tubes need to be preheated. Even though a lot of experience has been gained in recent years on the operation of solar tower power plants, only few literatures exists on the subject of solar preheating. The experiences of three former demonstration solar power plants, named MSEE, Thémis and Solar Two form the major part of the literature on the topic of solar preheating. Within the MSEE Project and the Thémis Project, the preheat strategy was documented in detail for a cavity receiver [4] [5] [6]. Since this type of receiver exhibits a different thermal behavior compared to the HPMS-II test receiver, the preheat strategy cannot be compared to the strategy that must be developed for an external receiver, which is the state-of-the-art in commercial power plants, and which is also used in the HPMS-II Project. In contrast to the other two demonstration power plants, the preheating of the Solar Two project was documented for an external receiver [7]. For the reason of better comparability, the preheat strategy of the Solar Two project will be discussed in more detail. According to Vant-Hull [8] [9] and Pacheco [7], the basis of the preheating of the Solar Two Project was an algorithm that calculated the solar flux density to be applied as a function of the receiver temperature, with the goal of reaching a receiver temperature of 260 °C.

The preheat process started by imposing a flux density of 16-20 kW/m². With the duration of the heating process and the resulting temperature increase, the solar flux density was changed every 5 minutes by focusing a new array of heliostats. The target was a final flux density between 12 to 36 kW/m², depending on thermal losses. When high convection losses occurred, the target temperature could not be reached with the predefined algorithm. This led to the fact that the molten salt began to crystallize at the junction between the electrically and solar heated tubes during the

filling of the receiver. In order to prevent this for the subsequent warm-up processes an operator had to control individual heliostats in addition to the control system. Moreover, preheating proved to be difficult in the early morning, when the elevation angle is below 10°. Due to its rapid increase, the selected heliostats generated two to twelve times the allowed flux density. For this reason, the number of heliostats had to be reduced by 20 % within a very short period of time in the morning. When the target temperature of 260 °C was reached, the receiver was filled. Further focusing of the heliostats followed in a 5-minute cycle until all were aligned. The preheat process took 15 minutes in total. The thermal stress and fatigue damage of the central receiver tubes during their preheating with the Vant-Hull algorithm was investigated. It could be determined that the Vant-Hull algorithm does not compromise the structural integrity of the studied receiver tubes [10]. However, no allowable temperature ramps were considered in this preheating process.

RECEIVER

The geometry of the HPMS-II test receiver is based on the design of a commercial external receiver. It is a tubular molten salt receiver that consists of 16 absorber tubes welded to the header via connecting tubes of the same diameter. The engineering of the receiver allows a serpentine flow of the solar salt with a receiver mass flow range between 1.3 to 12.8 kg/s and allows the operation at incident solar flux density up to 1000 kW/m² [3]. The absorber tubes are made of the austenitic steel DMV310 N. This material is designed for the use in high temperature areas and it shows high corrosion resistance [11]. Upper and lower header and connecting tubes are completely covered with insulation that shields from direct solar irradiation. The absorber tubes are embedded in the insulation up to the half of their diameter. This protects the lateral tubes from being directly irradiated, which prevents overheating and severe bulging of the lateral tubes (**TABLE 1** and **FIGURE 1**).

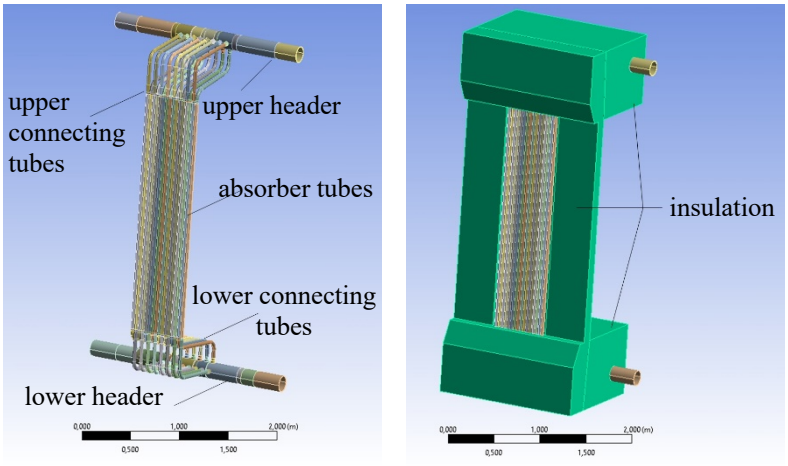

TABLE 1. Layout test receiver [3].

Feature	Value
Thermal rating	1 MW_{th}
Tube outside diameter	36.8 mm
Maximum flux density	1000 kW/m²
Tube wall thickness	2 mm
Absorber tube lengths	2.5 m
Number of absorber tubes	16
Number of serial tubes	8

FIGURE 1. ANSYS model of the receiver without (a) and with (b) the insulation.

All pipes, apart from the absorber tubes, are heated up electrically by using conventional resistance heaters that are wrapped in a meandering pattern. The absorber tubes receive a Pyromark coating to increase the absorption level [12]. According to the producer of the coating, the heating rate of Pyromark is limited to 30 K/min. Furthermore, due to the use of solar salt as a heat transfer medium, which has its crystallization point at 240 °C [1], a target temperature of 350 °C for preheating was defined.

PREHEATING CONCEPT

The basic concept of the solar preheating of the Solar Two project was adapted for the preheating concept of the HPMS-II receiver. As already shown for the Solar Two receiver, the allowable preheating solar flux density is dependent on the receiver temperature. In contrast to the algorithm used in Solar Two, maximum temperature ramps specified by the coating manufacturer must be implemented as an additional boundary condition. The following measurement data is available to monitor the preheating process: the incident solar flux is measured using eight flux gauges placed directly next to the absorber tubes. In addition, the absorber backwall temperatures are measured by

thermocouples. This data shall be used to control the preheating process. For this purpose, a relation between the number of used heliostats at a certain moment of the year and the resulting heating rate must be deduced.

SIMULATION

The development of the preheat strategy is based on two different simulation models. On one hand, an optical model of the Jülich heliostat field is developed based on the ray tracing software SPRAY [13]. On the other hand, a transient thermal FEM model of the HPMS-II receiver is developed using ANSYS Mechanical APDL. The goal of the optical simulations is to determine a relationship between the heliostats to be focused depending on the day of the year and the time of the day in order to achieve a certain solar flux density on the receiver. The goal of the thermal simulations is to develop a correlation that represents the maximum allowable preheat solar flux density as a function of the measured backwall absorber tube temperature. By combining the results of both simulations, it is possible to determine how the temperature of the receiver is affected by focusing certain heliostats.

Optical Simulation

The solar flux density is the result of the concentrating of the solar radiation by the heliostats. It depends among others on the intensity of the solar radiation (the DNI), on the number of focused heliostats and lastly on the heliostat field performance, which in turn depends on the day of the year and the time of the day. To develop a preheating strategy, which is independent of the day of the year and time, the correlations of the optical influences on the solar flux density are determined with the help of the raytracing model. To be able to simulate the incident solar flux density in the raytracing software, the position of all components of the Jülich tower power plant must be implemented (**FIGURE 2**). Furthermore, the optical influences affecting the heliostat field must be considered. An overview of the main assumptions taken for the raytracing simulation are shown in **TABLE 2**.

TABLE 2. Input heliostat field

Input for heliostat field	Value
Number of aim points on receiver surface	1
Number of heliostats	2065
Number of facets of each heliostat	4
Mirror slope error	0.00115
Error in rotation of tracking axes	0.002
Reflectivity of the mirror	0.89

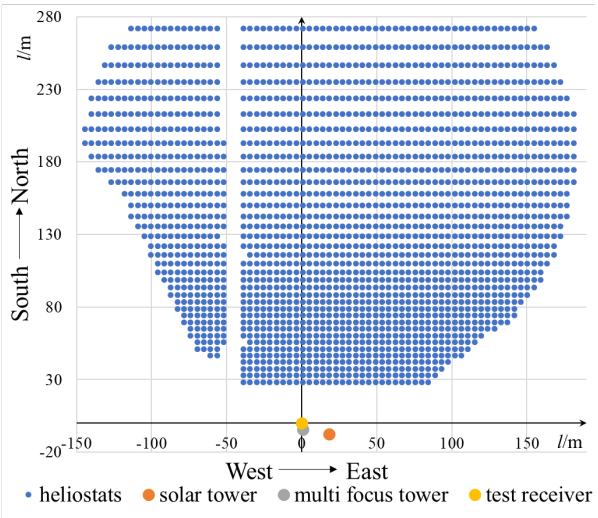

FIGURE 2. Heliostat field in Juelich.

As flux densities well below 50 kW/m² are required to reach the desired preheating temperatures, only a part of the whole heliostat field is needed (600 heliostats). To obtain a homogenous solar flux density distribution and hence a homogenous temperature distribution, the rear heliostats are selected as they exhibit a long focal length and thus project larger images on the receiver surface. For further calculations, the incident solar flux density on the receiver aperture $\dot{q}_{\mathrm{SF}}$ as a function of the number of heliostats is computed for two different seasons: June (summer) and February (spring). **FIGURE 3** shows the results. With the increase of the number of heliostats a linear increase of the solar flux density, that is shown on the y-axis, occurs. This is important, as this linear correlation allows relevant simplifications later on. The differences of the slope of the graphs are due to the different optical losses that apply to the variation of the simulated season. It can be seen that a flux density of f.ex. 20 kW/m² is reached using roughly 100 heliostats in Clear sky conditions at 12:00 in June, whereas roughly 600 heliostats are necessary to reach the same

heat flux at 08:30 in February. Hence the number of required heliostats strongly varies with the time of the day and day of the year.

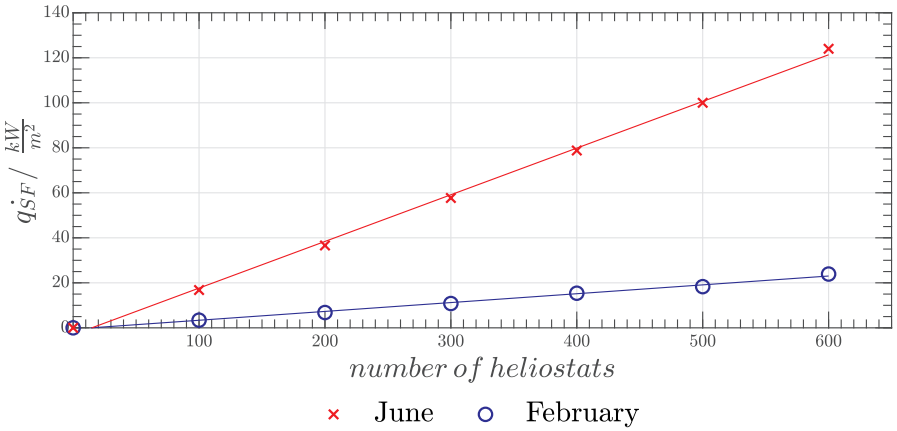

FIGURE 3. Relationship between the solar flux density and the number of heliostats for Clear Sky DNI for two exemplar dates 21.06. at 12:00 and 24.02. at 07:30 (Solar time).

Blocking, shading and the cosine effects highly depends on the position of the sun and thus on the azimuth angle and the elevation [13,14]. In order to account for these losses over the year, the following scaling factor is defined.

$$R_s = \frac{\dot{q}_{\mathrm{SF\,elevation\ \theta\ ,azimuth\ \gamma}}}{\dot{q}_{\mathrm{SF\,elevation\ 62{,}5°,azimuth\ 0°}}} \tag{1}$$

In this formula, the incident solar flux density at the receiver for an elevation θ and azimuth angle γ, is compared with an incident solar flux density at the receiver in a reference condition. The reference condition is summer solstice at solar noon. **TABLE 3** shows the result of the calculated scaling factor using the raytracing model. Above an elevation angle of 35° and an azimuth angle of 30° no difference between the incident flux density and the reference flux density is detected. In these cases, all scaling factor amounts to one and are not displayed in this paper.

TABLE 3. Scaling factor R_s depending on elevation and azimuth angle.

Azimuth angle γ / °	**Elevation θ / °**						
	5	**10**	**15**	**20**	**25**	**30**	
-120	0.65	/	/	/	/	/	/
-110	0.76	0.91	/	/	/	/	/
-100	0.85	0.70	0.77	0.84	/	/	/
-90	0.24	0.49	0.69	0.77	0.88	0.95	/
-80	0.48	0.57	0.55	0.86	0.91	1.00	0.98
-70	0.70	0.72	0.80	0.87	0.96	0.98	1.04
-60	0.80	0.92	0.94	0.97	1.00	1.05	1.05
-50	0.89	1.07	1.03	1.05	1.10	0.99	1.03
-40	0.88	1.03	1.03	0.98	1.00	1.03	0.99
-30	/	0.96	1.03	0.97	1.03	1.01	1.03

Using the scaling factor R_s, a correlation between a goal incident solar flux density at the receiver $\dot{q}_{\mathrm{SF,GOAL,\gamma,\theta}}$ and the number of necessary heliostats can be defined:

$$number_{\mathrm{Helio\ necessary,\gamma,\theta}} = n_{\mathrm{Helio\ necessary,REF}} \cdot \frac{DNI_{\mathrm{clear\ Sky,REF}}}{DNI_{\mathrm{clear\ Sky,\gamma,\theta}}} \cdot \frac{1}{R_s} \cdot \frac{\dot{q}_{\mathrm{SF,GOAL,\gamma,\theta}}}{\dot{q}_{\mathrm{SF,GOAL,REF}}} \tag{2}$$

With this formula, the number of necessary heliostats in order to achieve a certain incident solar flux density at the receiver at an elevation θ and an azimuth γ is calculated based on a reference case for which the relation between

solar flux and number of necessary heliostats in known. This can be done because of the roughly linear correlation between number of heliostats and incident solar flux. In the case of the HPMS-II receiver, the reference conditions at Solar Noon on 21st June was chosen: this results in a $DNI_{\text{clear Sky,REF}}$ of 810 kW/m² according to Hottel [15]. Furthermore, a goal reference flux density of $\dot{q}_{\text{SF,GOAL,REF}}$ =3 kW/m² was chosen arbitrarily. Simulations, showed that in the chosen reference conditions $n_{\text{Helio necessary,REF}} = 11$ heliostats are needed to achieve $\dot{q}_{\text{SF,GOAL,REF}}$. As DNI, Clear Sky DNI on the basis of the Hottel correlation [15] is assumed, in order to always maintain a conservative DNI estimation. This might lead to slower but therefore safe preheating rates. The input of the desired flux density depends on the receiver temperature and is limited by the boundary condition of the maximum temperature ramp of 30 K/min; which will be shown in the "Thermal simulation" section.

Thermal Simulation

For the thermal simulation, the receiver geometry was implemented in ANSYS as shown in **FIGURE 1**. The thermal radiative exchange between the absorber tubes and the insulation as well as the radiation to the ambient is modeled using the radiosity method. The natural and forced convection losses to the ambient are modeled using heat transfer coefficients. The material properties of the receiver and the insulation are implemented in order to achieve a transient model of the receiver. The local heat transfer at the inside of the tubes to the air inside the tubes is neglected. The solar preheating strongly depends on the occurring thermal losses. Therefore, a study of historic weather data, collected in the last three years, with the weather station on the Solar Tower in Jülich was performed in order to deduce common ambient temperatures and wind speeds for all four seasons. The results of this study can be found in **TABLE 4**. Based on the assumed ambient conditions, the corresponding heat transfer coefficient was calculated using Churchills correlation for a vertical plate [16]

TABLE 4. thermal boundaries for different models of thermal losses.

Name of model	Ambient temperature /°C	Wind speed/ m/s	Corresponding heat transfer coefficient/ W/(m²*K)
Extremely low thermal losses	40	0	8
Summer	20	2.8	13
Spring/ Autumn	15	6.9	26
Winter	5	10.6	42

Only one aim point is assumed for the HPMS-II test receiver during preheating, which leads to an inhomogeneous flux distribution. As a consequence of the profile, higher temperature gradients will occur. Therefore, this profile must be considered within the thermal simulation. The solar flux density profile, emerging from the optical simulation, is applied as a boundary condition onto the thermal FEM model - see **FIGURE 4 (a)**.

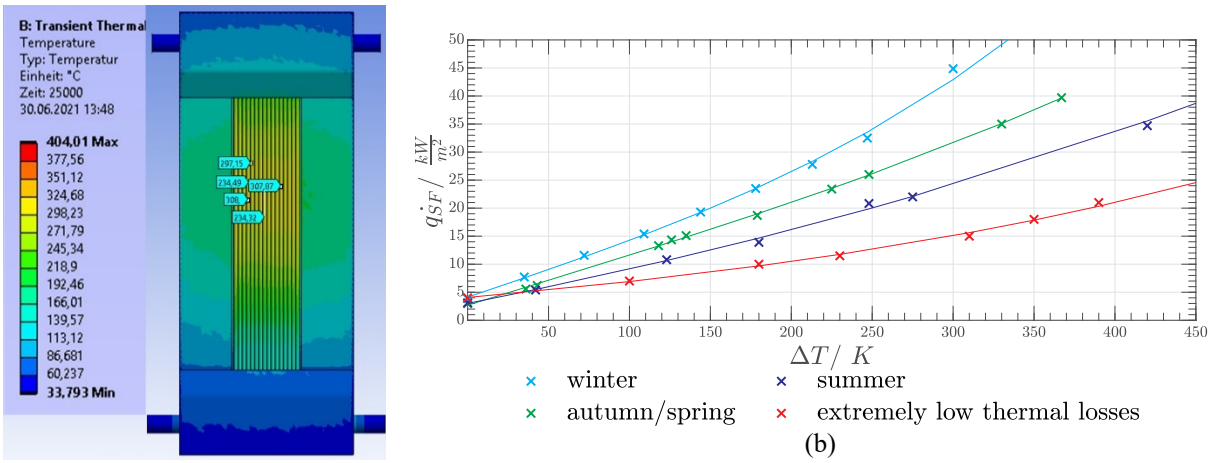

FIGURE 4. solar flux density profile on the receiver's surface (a) and maximum allowable flux density as a function of the difference of the temperature of the receiver and the ambient (b).

For the calculation of the number of heliostats to be focused $number_{\text{Helio necessary},\gamma,\theta}$, the desired flux density $\dot{q}_{SF,GOAL,\gamma,\theta}$ must be determined. The desired flux density represents the maximum allowable flux density on the receiver so that the temperature ramp is maintained. This maximum allowable flux density is temperature-dependent and is therefore a function of the difference between the ambient and the receiver temperature $\Delta T=T_{rec}-T_{amb}$. Using an iterative process, the thermal transient model was used to deduce the incident solar flux density $\dot{q}_{SF,GOAL,\gamma,\theta}$ necessary to maintain a temperature transient of 30 K/min. **FIGURE 4 (b)** shows the resulting incident solar flux as a function of temperature gradients between receiver and ambient for all 4 defined boundary conditions. The higher the thermal losses and the higher the temperature difference, the greater is the maximum allowable flux density.

SOLAR HEATING PROCESS

With the results from the simulation, the solar heating process can be finalized. The process consists of three steps. The first step is that the operator chooses the thermal model, depending on the ambient conditions. In a second step the algorithm calculates the maximum number of heliostats. Input for this calculation is the elevation and azimuth angle of the sun, the measured absorber temperature and the measured ambient temperature. Based on the measured receiver backwall temperature and the ambient temperature, the maximum allowable solar flux is computed. Then the algorithm calculates the Clear Sky DNI and the scaling factor R_s depending on the elevation and the azimuth angle. With the help of **FORMULA 2**, with the inputs of the previously determined DNI, scaling factor, and maximum allowable flux density, the maximum number of heliostats is determined. During the preheating process, the operator must monitor the time dependent course of the solar flux density and the temperature and will then decide in the third step how many of the algorithm's proposed heliostats should be focused. **FIGURE 5** illustrate the procedure.

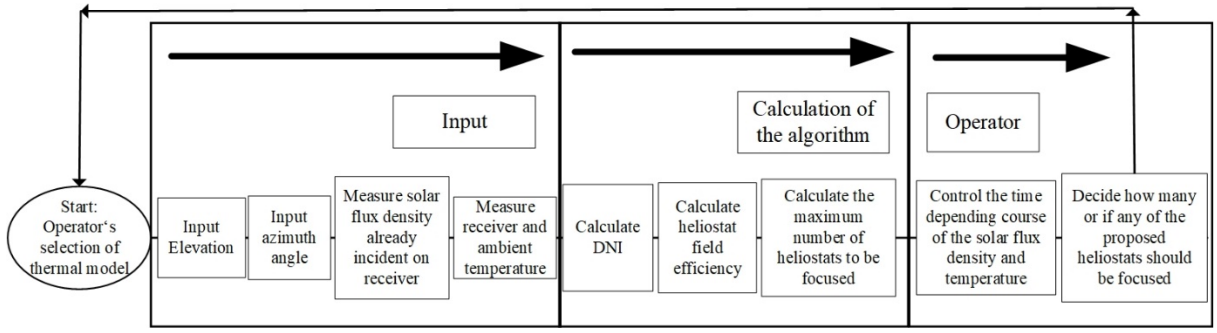

FIGURE 5. Procedure of the solar heating process.

FEASIBILITY TEST

The feasibility of the developed preheat strategy is demonstrated in the course of the work based on two different simulations examples. It is to be checked which temperature transients occur during preheating, whether the target temperature can be reached and how long the solar preheating will take. In order to be able, to simulate solar heating with the thermal model, the flux densities must be defined as a function of time. For the simulation, an exemplar number of heliostats will be set. Also, the times at which the flux densities are increased are set arbitrarily. This can lead to the fact that that the defined temperature ramp of 30 K/min is not maintained in the present example. However, for the purpose of demonstrating the feasibility of the preheating strategy, it is not important that the temperature ramp is maintained during the simulation; the goal of this demonstration is to show that the preheating strategy would detect the exceeding of the temperature ramp. A high risk of overheating the receiver occurs during the strongest temporal variation of solar flux density in combination with low thermal losses of the heating process. In addition, it will be difficult to maintain the temperature ramp. The highest temporal change of the solar flux density in Jülich occurs on the 29.03. at 08:30 a.m. (local time). Thus, the simulation of solar preheating should be performed for this day under consideration of low thermal losses. For the simulation, three-time steps in which the solar flux density is increased, were defined. At these timestep an arbitrary increase of the flux density was determined. With the help of **FORMULA 2**, the resulting number of heliostats was calculated. In order to demonstrate the validity of the formula, the number of focused heliostats was implemented in the optical model SPRAY and it was checked whether the pre-defined solar flux density is the same as the resulting flux density from the optical simulation. The results are shown

in **TABLE 5**. The flux densities agree well for this example: The maximum deviation is roughly 1 kW/m² which is acceptable.

TABLE 5. Calculated flux density compares with simulated flux density.

Time	Defined desired flux density/ kW/ m²	Number of Heliostats	Simulated desired flux density
08:30 a.m.	3.2	105	3
08:35 a.m.	7.7	193	7.5
08:40 a.m.	11.2	270	12.3

Using the thermal FEM model, the temperature of the receiver's absorber tubes and the occurring temperature transients are simulated. For this purpose, the defined flux density as a function of time (cf **TABLE 5**) and the solar flux density profile, shown in **FIGURE 4 (a)**, were implemented. The result of the thermal simulation is shown in **FIGURE 6**: The simulated absolute temperature (right ordinate) and temperature transient (left ordinate) are shown as a function of the duration of the preheating. The red graph indicates the temperature profile on the front of the tubes and the blue graph shows the temperature profile on the back of the tube. As expected, the tube temperature increases with time and the temperature level of the rear side of the tube is always below the temperature level of the front side. The temperature gradients between the front and back of the absorber tube increase with time and amount to a maximum of 140 K after 25 minutes. In this simulation the preheating of the tube is concluded after 17 minutes.

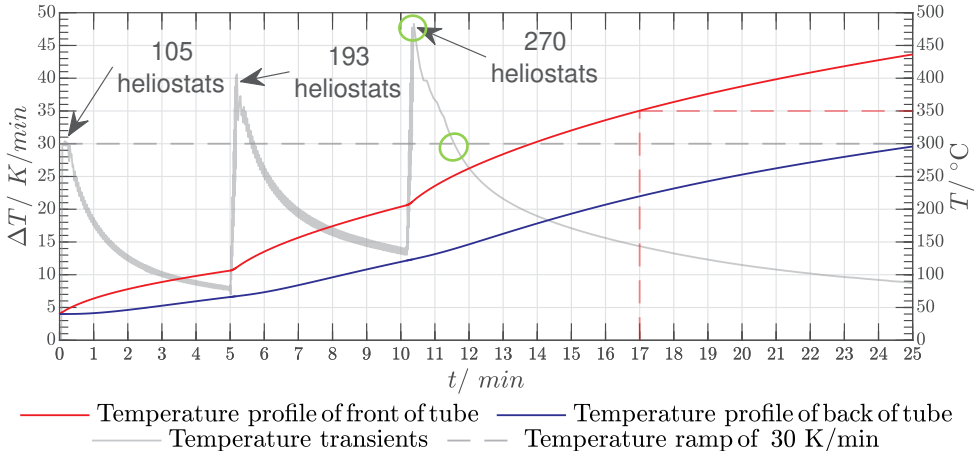

FIGURE 6. Occurring temperature and temperature transients depending on the preheat duration.

The grey graph in **FIGURE 6** shows the occurring temperature transients at the position of the maximum temperature: indeed, the defined maximum temperature ramp of 30 K/min can be maintained for the first number of focused heliostats. However, at the second increase in number of heliostats, the temperature transients amount up to 40 K/min and up to 50 K/min with the 3rd increase. In order to check whether the exceeding would have been noticed during preheating, the course of the solar flux density during the simulation is compared with the maximum allowable flux density course that is calculated by the developed relationship respecting low thermal losses, shown in **FIGURE 4 (b)**. The temperature difference between the ambient and the absorber tube, that represents the input for this relationship, can be taken from the result of the thermal simulation. The following relationship could be determined. The areas that marked by green circles are examined in detail in further course of the paper as a part of the mechanical analysis.

In **FIGURE 7** the red line represents the theoretical course of the maximum permissible flux density (compare section "thermal simulation"). The green line shows the actual course of the occurring solar flux density from the simulation. Compared to **FIGURE 6**, the compliance of the temperature ramp at the beginning as well as the exceeding of the temperature ramp after the 2nd and 3rd increase is correctly recorded. Thus, it could be proven that during preheating the exceeding of the temperature ramp would have been noticed and the operator could have intervened to prevent this situation. In total the preheating takes 25 minutes. Since the preheating was simulated on the basis of low thermal losses, it can be expected that preheating is going to take more time, taking into account higher thermal losses. To

estimate how long the preheating will take, in consideration of high thermal losses, a simulation was made under thermal losses that represent the season spring/autumn boundary conditions (compare **TABLE 4**).

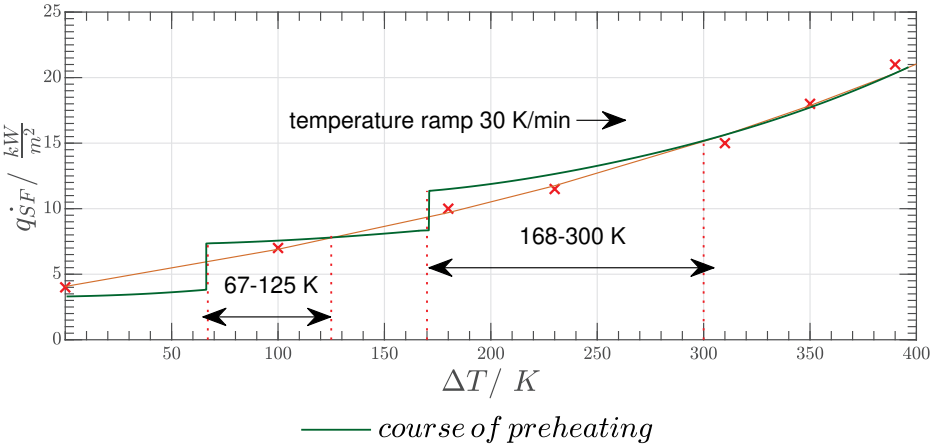

FIGURE 7. Comparison of the maximum allowable flux density and the actual occurring flux density.

The procedure for this simulation is the same as the previous thermal simulation, except that this simulation was repeated and adjusted iteratively until the temperature ramp was maintained for each increase in solar flux density. The result of the simulation can be taken from the following **FIGURE 8**.

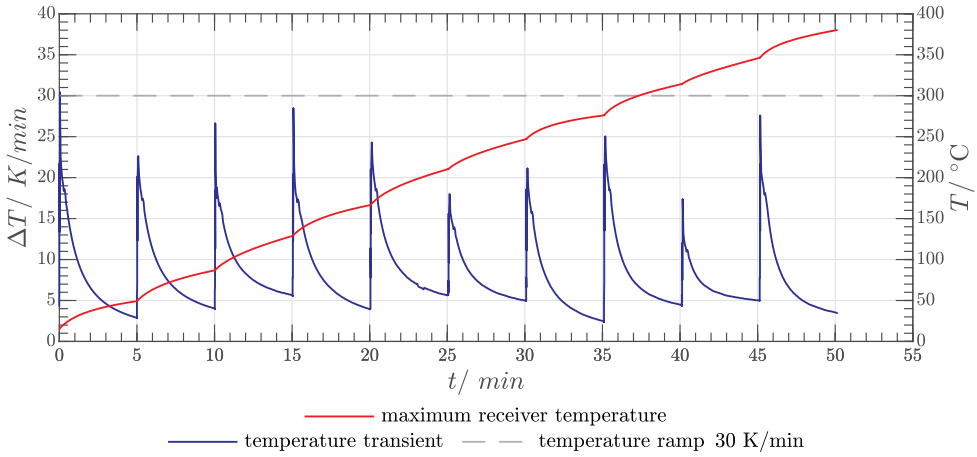

FIGURE 8. Duration of solar preheating considering higher thermal losses.

The x-axis shows the duration of the preheating in minutes. The ordinate on the left displays the temperature transients in K/min and the one on the right side the temperature in °C. The red line represents the rising temperature of the receiver. The blue line shows the occurring temperature transients. To reach the target temperature of 350 °C, a preheating time of 50 minutes is necessary in this case. The main reason for the long duration of solar preheating is the requirement of the coating manufacturer to maintain the temperature ramp of 30 K/min. In order to determine whether it is possible to develop a less time-consuming preheating, which would, however, lead to higher temperature transients, the structural-mechanical consequences of a preheating with exceeding of the temperature ramp are determined in the next section.

MECHANICAL ANALYSIS

In addition to the maximum temperature ramp, defined by the coating manufacturer, this chapter examines the damage of the absorber tubes themselves by the preheating process. Based on the thermal simulations described above, the fatigue damage for the prototype receiver is calculated for selected load cases. In addition, the damage is scaled

up to 30 years of operation in order to be able to evaluate the transferability of the preheating process to commercial power plants. For the evaluation of the damage, two different load cases are considered (cf. **FIGURE 6**):

- Load case A: Temperature ramp of 50 K/min at a flux density of 12.37 kW/m²; the maximum tube temperature is scaled up from 210 °C to 350 °C.
- Load case B: Temperature ramp of 30 K/min at a flux density of 12.96 kW/m²; the maximum tube temperature is scaled up from 250 °C to 350 °C.

The temperature is increased to the desired target temperature of 350 °C in both cases, since this is the more critical case for evaluating the damage. For the evaluation, 1000 load cycles are assumed, as in the receiver design (cf. [3]). The evaluation itself follows the creep-fatigue approach in ASME BPVC Section III Division 5, in which the influence of creep is negligible due to the comparatively low operating temperatures [17]. For the evaluation of the fatigue damage, the occurring strain is the decisive parameter. **FIGURE 9** shows an example of the total strain intensity calculated by the finite element method for load case B. The tubes are irradiated from the bottom side of the figure. As expected, the maximum strains occur there.

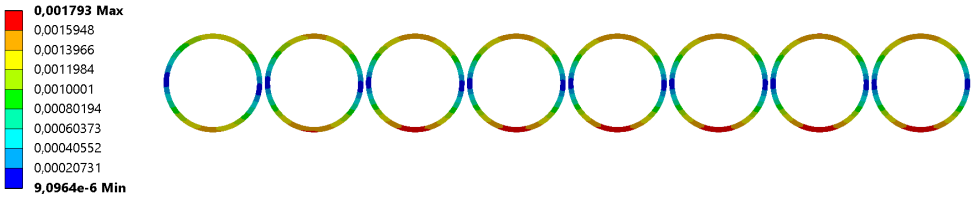

FIGURE 9. Calculated strain of eight exemplary absorber tubes irradiated from the bottom side.

TABLE 6 shows the damage for both load cases and all calculated paths (across the wall thickness at the irradiated side of the three different absorber tubes). The fatigue damages are on a very low level, so that the preheating process can be evaluated as uncritical for the lifetime of the absorber tubes. The calculated damage is at the highest level for the boundary conditions of load case B. This is particularly visible in Path_02, where a damage greater than 0.0 % is calculated. If, for the calculated strains, the damage calculation is scaled up to 30 years of operation and 10950 preheating cycles, the maximum damage is 1.7 %. This value is rather high, but it is considered to be acceptable due to the conservative load case considered (high temperature difference at maximum absorber tube temperature).

TABLE 6. Fatigue damage calculated for the prototype receiver.

location	Path_01	Path_02	Path_03
fatigue damage load case A	0.0 %	0.0 %	0.0 %
fatigue damage load case B	0.0 %	0.2 %	0.0 %

Thus, for the calculated fatigue damage of the absorber tubes, not the maximum temperature ramp (cf. load case A), but the highest temperature difference (cf. load case B) over the absorber tubes is decisive. The permissible temperature difference decreases with increasing tube temperature. If it is also considered that, for reasons of operational safety, the ideal heating process should end in a constant tube temperature. The following preheating strategy appears to be ideal in terms of the absorber tubes. During preheating, the incident flux density can be increased comparatively fast, then kept at a high level and slowly reduced again before the target temperature is reached. On the one hand, this procedure exceeds the given limit for the heating rate significantly. On the other hand, solar receivers also see significantly larger temperature rates than 30 K/min during solar operation, for example, when clouds pass through. Thus, the limit of the heating rate can be understood as a recommendation, whose exceeding contributes to accelerated material aging, but not as an absolute limit.

CONCLUSION AND OUTLOOK

The demonstrated preheating strategy leads to safe start-up operation of the test receiver. By using an optical simulation based on raytracing, a relationship correlation was developed between the number of focused heliostats and the resulting solar flux density incident on the receivers' surface, considering the position of the sun. To ensure that the temperature ramp of 30 K/min is not exceeded, a thermal simulation was used to determine a relationship

between the receiver temperature and the maximum allowable flux density, considering thermal losses, which depend on the ambient temperature and the wind speed. By combining the results of both simulations, a preheating strategy was defined that calculates the maximum number of heliostats to be focused based on the receiver temperature, ambient conditions, and the position of the sun to maintain the temperature ramp until the target temperature is reached. In addition, the fatigue damage during preheating was calculated. It was found, that not the maximum temperature ramp but the highest temperature difference over the absorber tubes is decisive. The mechanical calculation shows a possibility for time optimization of the preheating process. However, this conflicts with the given limit for the heating rate of coated absorber tubes, so that ultimately an economic optimization from the duration of the preheating process and material damage (coating and metal tube) is necessary.

ACKNOWLEDGMENTS

This work has been funded by the “German Federal Ministry for Economic Affairs and Energy” as well as by the “Ministerium für Wirtschaft, Innovation, Digitalisierung und Energie des Landes Nordrhein-Westfalen.

Bundesministerium für Wirtschaft und Energie

Ministerium für Wirtschaft, Innovation, Digitalisierung und Energie des Landes Nordrhein-Westfalen

REFERENCES

1. E. Zarza Moya, Innovative working fluids for parabolic trough collectors, Advances in Concentrating Solar Thermal Research and Technology, 2017
2. A. Bonk et al., Solar Salt - Pushing an old material for energy storage to a new limit, Applied Energy 262, 2020
3. C. Frantz et al., Basic Engineering of a High Performance Molten Salt Tower Receiver System (SolarPACES 2020)
4. A. Amri, I. Izygon, and B. Tedjiza, Central Receiver Plant Evaluation, III) Thesis Receiver subsystem evaluation, Sandia National Laboratories, Livermore and California, 1987,
5. D.C. Smith, and J.M. Chavez, A FINAL REPORT ON THE PHASE TESTING OF A MOLTEN_SALT CAVITY RECEIVER, A Summary Report, Sandia National Laboratories, Albuquerque, 1988
6. R.J. Holl., D.R. Barron, and S. Saloff, Molten Salt Solar-Electric Experiment in Testing, Operation and Evaluation, Electric Power Research Institute, California, 1989
7. J.E. Pacheco, Final Test and Evaluation Results from the Solar Two Project, Sandia National Laboratories, Albuquerque, 2002
8. L.L. Vant-Hull, The Role of "Allowable Flux Density" in the Design and Operation of Molten-Salt Solar Central Receivers, Solar Energy Engineering 124, 2002
9. L. L. Vant-Hull, M.E. Izygon, and C.L. Pitman, REAL-TIME COMPUTATION AND CONTROL OF SOLAR FLUX DENSITY ON A CENTRAL RECEIVER (SOLAR TWO), Solar Engineering, 1996
10. R. Pérez-Álvarez et al., Thermal stress and fatigue damage of central receiver tubes during their preheating, Applied Thermal Engineering 195, August 2021
11. S. Giuliano et al. (2016), High Performance Molten Salt Tower Receiver System, Final Report, Germany
12. C.K: Ho et al., Characterization of Pyromark 2500 Paint for High-Temperature Solar Receivers, Journal of Solar Energy Engineering 136, 2014
13. R. Buck, Solar Raytracing Tool SPRAY-User Manual, D.Z.f.L.u. Raumfahrt, 2011, Stuttgart
14. Weinrebe, G., Technische, ökologische und ökonomische Analyse von solarthermischen Kraftwerken, 2000, Universität Stuttgart
15. A. Islahi, S. Shakil, and M. Hamed, Hottel's Clear Day Model for a typical arid city-Jeddah, International Journal of Engineering Science Invention, 2015. 4(6): p. 32-37.
16. S.W. Churchill and H.H.S. Chu, Correlation Equations for Laminar and Turbulent Free Convection from a Vertical Plate, International Journal of Heat and Mass Transfer 18: p. 1323-1329 , 1975
17. American Society of Mechanical Engineers, ASME Boiler and Pressure Vessel Code - Section III Rules for Construction of Nuclear Facility Components - Division 5-High Temperature Reactors (2019)